Proceeding of the 7th International Symposium on Artificial Intelligence, Robotics and Automation in Space: i-SAIRAS 2003, NARA, Japan, May 19-23, 2003

# A ROBOTIC ARM FOR ON-GROUND VALIDATION OF AUTONOMOUS NAVIGATION ALGORITHMS

A.Davighi (davighi@aero.polimi.it), F.Bernelli-Zazzera (Franco.Bernelli@polimi.it)
*Dipartimento di Ingegneria Aerospaziale, Politecnico di Milano, Milano*
*Via La Masa 34,20156 Milano,Italy*

## ABSTRACT

In this paper a robotic arm for ground testing autonomous navigation algorithms is presented.
The aim is to design and build a robotic arm to be used for simulation of space trajectories, like fly-by and landing of probes, and in general approach trajectories to celestial bodies. This system will be used in the future as a ground based laboratory for the design and validation of autonomous navigation algorithms .

## 1.INTRODUCTION

Future missions to explore planets, asteroids, comets will involve autonomous spacecraft, and should include not only an orbiting phase, but also a landing phase to gather actual samples.
Autonomy is becoming a driver for near future projects, in fact autonomy reduces the need for support from ground, so reducing ground station development and maintenance, cost, man effort and in particular reaction time to unexpected situations, avoiding dangerous delays in control loops. Next generation landers, destined to interplanetary exploration, are excellent examples for which autonomy is a mandatory capability: they are designed to operate far from Earth in unknown an hostile environments, with a big delay in transmission time of commands. Historically navigation is completely demanded to operations on Earth, with a consequent cost in terms of human resources and to the fundamental issues related to the delay in receiving and sending signals to and from the spacecraft or related to possible occultation or failure that may jeopardise the entire mission.
For landing operations, one of the driving issue is to avoid obstacles during descent and to break in time for a soft touch-down.
ESA is performing landing missions since few years, such as ARD (completed mission), Huygens (mission in progress), Roland (DLR), Beagle (BNSC), Bepi Colombo (approved missions).
Due to the communication round trip delay and the rapid response time needed, lander missions often need to be autonomous to some degree. Planetary lander missions are also characterized by high delta V requirements, leading to low payload mass fractions. As the prime mission objective for landers may be summarized as: "the safe delivery of a given payload mass to the surface", the mass fraction taken by the avionic system needed to achieve a safe landing has to be minimized. More so, as the avionic system often do not have any function after completion of the landing. The systems studied by ESA for the fullfillment of these requirements include passive and active optical sensors, radars, atmospheric entry with hypersonic steering, and various low speed atmospheric landing techniques.
Given the above mentioned scenario, it is very important to be able to perform the experimental validation of autonomous navigation alghoritms and for the simulation of probe landings on the surface of celestial bodies or of particular space trajectories.
With this goal an experimental system has been realized, equipped with an optic videocamera (the ccd sensor of a webcam) in order to capture images of the environment and, particulary, the images of an object simulating the celestial body (for example a model of a planetary surface). The sensor is fixed to the tip of robotic arm. Moreover, it is desiderable to have the possibility of correcting the trajectory on the basis of the autonomous navigation algorithms (for example to avoid an obstacle).
We decided to adopt step-by-step motors instead of the common DC motors. The main advantage of this choice resides in the possibility of activating the same motors in open loop, in other words without feedback and therefore without the necessity of performing any measure. In particular, the motor control is achieved by means of signals received by electronic cards that are connected to the PC through the parallel port.
In section 3 we describes the main feature of a step-by-step motor which we utilize for move the robotic arm; in section 4 we propose a phase of mechanic structure selection and the phase of design of robotic arm links and selection of stepper motors; in section 5 and 6 we describes the robotic arm modelling and the control algorithm; in section 7 we present the simulation with a model of a generic celestial body surface.

## 2. THE ROBOTIC ARM DESIGN

The robotic arm mechanics structure can be either open or closed kinematics chain. In the former case every degree of mobility of the structure corresponds to a joint. In the latter case the relevant movement of two links induces relevant movements among other links.

The utilization of closed kinematics chains is mainly dictated by stiffness requirements.
The open kinematics chain undoubtedly has the advantages and economicity. For these reasons we have adopted a open kinematics chain geometry , also because of the low mechanicals loads that the manipulator should counteract. A fundamental performance that the robotic arm should guarantee is its work space. The work space of a robotic arm represents the portion of the environment in which the terminal of the manipulator ( also called end-effector) can move. The work space must be wide enough to include all trajectories to be verified.
Six degrees of freedom of the structure are a minimal requirement. Every extra degree adds redundancy in the manipulator motion. These redundancies allow to reach the same position and orientation with different configurations of the joints. We have separated the 6 degrees of freedom into 3 degrees for position and 3 for orientation. That is, we have subdivided the robot in two parts: an upstream part of 3 link (and 3 joints) that allow to reach a position of the space, and a downstream part, called wrist. With 3 joints, that allows the videocamera to take any orientation. In particular, we have chosen to use a spherical wrist (Fig.1), where the 3 joints have rotation axes that all intersect in a point.

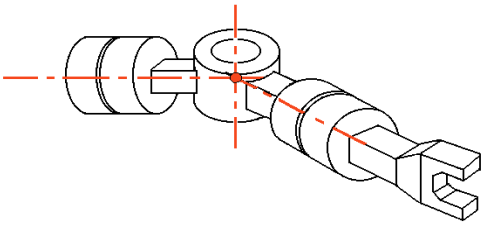

**Fig.1** -*The spherical wrist*

Therefore the fundamental advantage of a spherical wrist is the decoupling between position and orientation of the terminal effector . In fact, the supporting structure (the 3rd link) serves the task of positioning the intersection point of the wrist axes, while the configuration of the wrist joints determines the orientation of the terminal effector.
The goal is to realize a manipulator that allows to reproduce, with a certain skill, orbital trajectories (i.e. conical arcs ) or landing (i.e. trajectories where there is a main direction of movement and maybe small corrections along this main direction). We assumed that the landing should not be reproduced necessarily on the vertical, in fact we perceived immediately that a movement of the terminal camera of the manipulator (videocamera) is against gravitational force from all the bodies interested in a vertical movement. It is preferable therefore to reproduce trajectories with main direction in the horizontal plan. Even better if we choose the axis timely so as to allow to reach the differents points with the same balance.
Given these considerations, we selected two configurations that actually yield much more than our requirements. They are called anthropomophic manipulator and SCARA manipulator. The anthropomophic manipulator has the considerable advantage of using rotational joints exclusively, that offers greater simplicity, solidity and reliability. The SCARA manipulator allows a good vertical capacity of movements, but has the disadvantage of using a prismatic joint. At this point, to
have both the advantages of the anthropomorphic and SCARA manipulators, we selected the hybrid configuration show in fig.2.

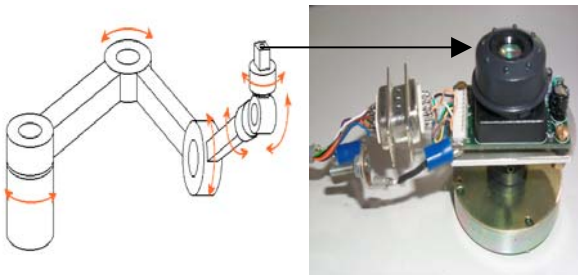

***Fig.2a*** *Hybrid manipulator-* ***Fig.2b-*** *Web-cam support and motor*

### 2.1 Links selection

To select the shape of the section we compared three different sections, reported in Fig.3 and Tab. 1, in terms of mass and overall stiffness in two different cases: the case of shear and bending and only twisting.

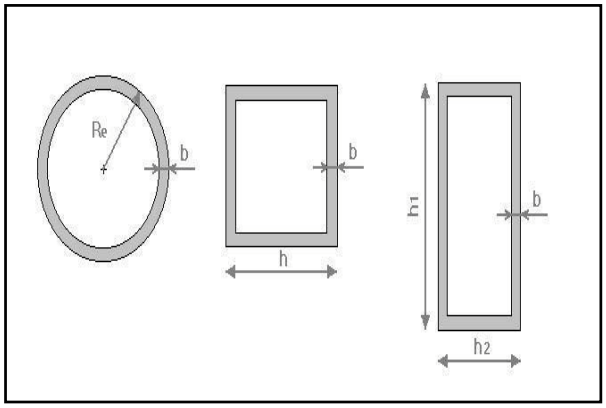


**Fig.3** - *Geometrical Features of the sections to comparison*

| | Circular section | | Square section | | Rectangular section |
|---|---|---|---|---|---|
| $R_e$ = [mm] | 40 | h = | 80 | $h_1$ = | 106.7 |
| b = [mm] | 5,173 | b = | 4 | $h_2$ = | 53.3 |
| | | | | B = | 4,3 |
| Area= [mm²] | 1216 | Area = | 1216 | Area = | 1216 |
| J = [$mm^4$] | 855136,1 | J = | 1173845 | J = | 1532412,46 |
| $I_p$ = [$mm^4$] | 1710272 | $I_p$ = | 1755904 | $I_p$ = | 1163336,4 |

**Tab.1** - *Features of three different sections to comparison*

We chose the square section, not only because it resists well to all loads, but also because allows to limit the vertical dimension of the link, characteristic rather important for the consideration on the interferences among the parts of the structure. The second choice pertains the material. We decided to use for the link construction a light alloy of aluminium (type 6060).
The aluminium thickness allows a great possibility of choice between the different thicknesses (of the order of the millimetres) to further optimise the design.
The links were then optimised in order to be subject to equal deformations. The final geometry is reported in Tab.2.

| Link | Lenght [cm] | Side [mm] | Thickness [mm] | Mass [Kg] |
|---|---|---|---|---|
| 1 | 40 | 80 | 4 | 1.313 |
| 2 | 40 | 60 | 3 | 0.739 |
| 3 | 30 | 50 | 2 | 0.311 |

***Tab.2*** *–Selected links dimensions*

**2.2 – Motor selection**

The joint motors are selected in the class of stepper motors, for ease of imposing the desired tip trajectory in open loop, considering the low tip loads.
The joints motors selection is based on the consideration that the constraint in terms of rotor inertia. Therefore after the motors and reduction gears selection we will verify that the load torque is lower than the limit motor torque.
Tab.3 reports all the features of the selected joints motors.

| Joint | Motor | Holding Torque [Nm] | Nominal Current [A] | R phase [Ω] |
|---|---|---|---|---|
| 1 | H31NRLT-LNN-NS-00 | 1.66 | 2.7 | 1.12 |
| 2 | H21NRLT-LNN-NS-00 | 0.60 | 1.39 | 2.8 |
| 3 | H2HNRLT-LNN-NS-00 | 0.36 | 1.26 | 2.89 |

| Joint | Motor | L phase [mH] | Rotor inertia [Kg m²] | Weight [Kg] |
|---|---|---|---|---|
| 1 | H31NRLT-LNN-NS-00 | 9.3 | $5.9 \cdot 10^{-5}$ | 1.45 |
| 2 | H21NRLT-LNN-NS-00 | 10.2 | $1.1 \cdot 10^{-5}$ | 0.55 |
| 3 | H2HNRLT-LNN-NS-00 | 7.3 | $7 \cdot 10^{-6}$ | 0.41 |

***Tab.3*** *–Selected motors features*

**2.3 – Reduction gears selection**

The main feature of a reduction gears should be its stiffness.
After an extensive analysis of many reduction gears, commercially available, the reduction gear family suitable to the constraints of our system appears to be the Harmonic Drive of the series HFUC, that with respect to other models guarantee the following advantages:

- high stiffness(particularly torsional);
- absence of stroke;
- high yield;
- excellent precision and accuracy on the positioning.

At this point we considered 5 different possible combinations of the reduction gears on three joints. In the following Tab.4 we compare the linear and angular deflection of end-effector and the total mass in the different configurations considered.

| Joint 1 | Joint 2 | Joint 3 | $\Delta_{tot}$ | $\delta_{tot}$ | Total mass reduction gears |
|---|---|---|---|---|---|
| HFUC 20 | HFUC 17 | HFUC 17 | 0.5474 [mm] | 0.0661 [°] | 2.26 [Kg] |
| HFUC 20 | HFUC 17 | HFUC 14 | 0.6189 [mm] | 0.0819 [°] | 2.11 [Kg] |
| ***HFUC 20*** | ***HFUC 14*** | ***HFUC 14*** | ***0.7169 [mm]*** | ***0.0896 [°]*** | ***1.96 [Kg]*** |
| HFUC 17 | HFUC 17 | HFUC 14 | 0.6777 [mm] | 0.0931 [°] | 1.77 [Kg] |
| HFUC 17 | HFUC 14 | HFUC 14 | 0.7742 [mm] | 0.1006 [°] | 1.62 [Kg] |

***Tab.4*** *– Deformation and mass of reduction gears*

**2.5 – Selection of wrist motors and reduction gears**

Tab.5 and 6 reports all the features of the selected wrist motors and reduction gears

| Nominal Voltage | Nominal Current | Phase Resistance |
|---|---|---|
| 9.6 [V] | 0.12 [A] | 80 [Ω] |

| Phase Inductance | Holding Torque | Step angle | Weight |
|---|---|---|---|
| 53 [mH] | 20 [mNm] | 1.8 [°] | 80 [g] |

***Tab.5*** *– Wrist motors features*

| Joint | Type | Reduction Ratio | Max Efficiency |
|---|---|---|---|
| 4 | 144043 | 128 (41553 / 325) | 59 % |
| 5 | 144039 | 84 (185193 / 2197) | 59 % |

| Joint | Type | Weight | Lenght $L_1$ |
|---|---|---|---|
| 4 | 144043 | 68 [g] | 42.8 [mm] |
| 5 | 144039 | 68 [g] | 42.8 [mm] |

***Tab.6-*** *Wrist reduction gears features*

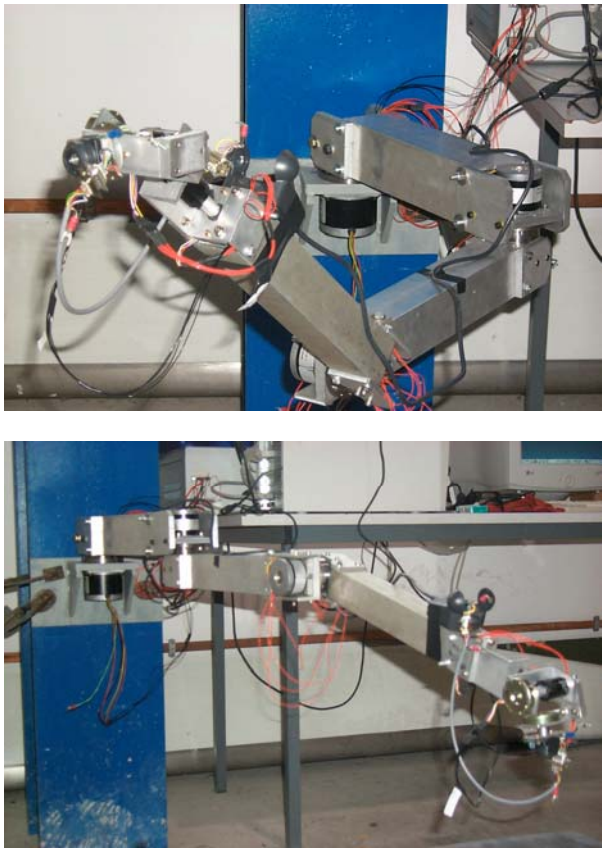

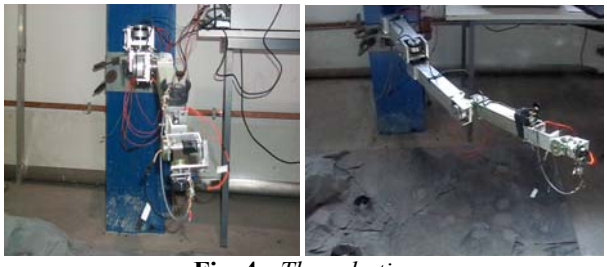

**Fig. 4** - *The robotic arm*

## 3 THE ROBOTIC ARM NUMERICAL MODEL

The numerical model of the robotic arm is built in order to simulate the direct dynamics and to evaluate the motor torques to perform given manoeuvres, using inverse simulation techniques.
The model is based on the assumption that all links are rigid, and no backlash in introduced by the motors and gears.
For both these purposes we used the Matlab Robotics Toolbox release 5 ([3]), that allows, to automate the calculation of direct and inverse kinematics.
We used a general and systematic method to define the rotations to impose to every joint to move the link end-effector, using the Denavit-Hartenberg's convention ([3]), reported in Tab.7

| | $a_i$ | $d_i$ | $\alpha_i$ | $\theta_i$ |
|---|---|---|---|---|
| i = 1 | $l_{b1}$ | 0 | 0 | $\theta_1$ |
| i = 2 | $l_{b2}$ | $-\Delta_{12}$ | $\pi / 2$ | $\theta_2$ |
| i = 3 | 0 | $-\Delta_{23}$ | $\pi / 2$ | $\theta_3 + \pi / 2$ |
| i = 4 | 0 | $l_3$ | $-\pi / 2$ | $\theta_4$ |
| i = 5 | 0 | 0 | $\pi / 2$ | $\theta_5$ |
| i = 6 | 0 | $l_{pulse}$ | 0 | $\theta_6$ |

***Tab.7*** *- Denavit-Hartenberg's parameters*

With the direct kinematics we calculate in unambiguous manner the end-effector position and orientation after the evaluation of the joints variable. On the contrary, the problem of inverse kinematics is more complex because the equations to solve are, in general, non linear. Therefore it is not always possible to find an analytic solution ( closed form solution); we can have multiple solutions; we can have infinite solutions ( redundant manipulator); or even no acceptable solution could be found, because of the kinematics structure of the manipulator.
The existence of solutions is guaranteed if the position and orientation assigned are in the manipulator work space.

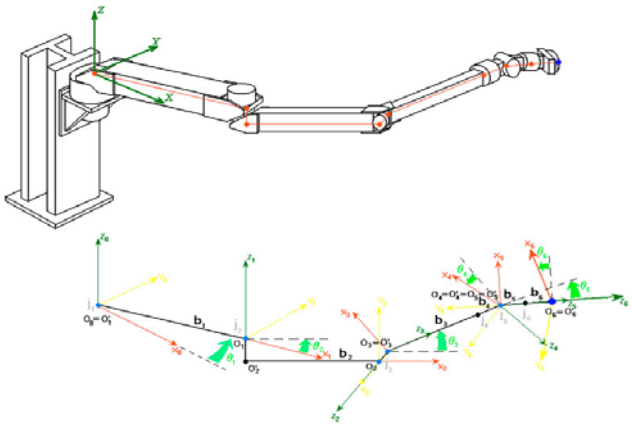

**Fig 5-** *Robotic arm scheme*

One example of simulate trajectories, for the scheme depicted in Fig. 5, is reported in Fig.6.

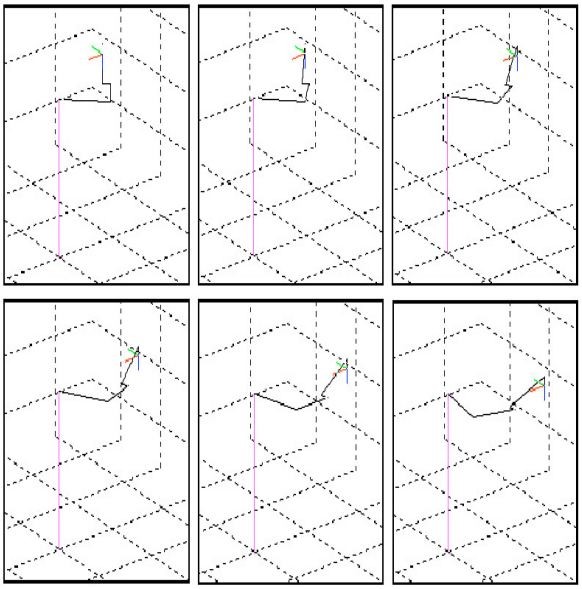

**Fig. 6**- Robot kinematics simulations with Matlab robotics toolbox

## 4. CONTROL ALGORITHM

The control algorithm, written for the robotic arm, allows to introduce a trajectory to reproduce specific orbits; or it allows to control the robotic arm with a feed-back , using the autonomous navigation algorithms that use a web-cam, fixed to extremity spherical wrist.
Using the autonomous navigation algorithms , we can simulate phases of vertical landing or with inclined trajectories, depending on the mission and therefore on the probe that we intend to simulate.
In this first phase we simulated in particular a vertical landing, controlling the horizontal and vertical movements via the web-cam that decided the movements of the robotic arm end-effector.
The procedure is completed in three main steps:

**Step 1: Acquisition of an image and windows identification of a zone suitable for landing.**
The process analyzes the image and decides the horizontal movement of the robotic arm, allowing therefore to correct the trajectory (for example to avoid the impact and to avoid an obstacle);
The vertical movements are instead prefixed at every step of the cycle as the arm lowers in order to simulate a constant vertical landing speed.

**Step 2: Evaluation of command signals for each motor.**
Given the trajectory that we want to reproduce we evaluate, with the inverse kinematics, the motion of each joint and we evaluate the command signals in terms of discrete time steps.
The trajectory, in the work space, is generated from Matlab with 6 vectors that reproduce the time progress of three cartesians coordinates and the three angles RPY of the end-effector orientation .

**Step 3: Generation, on the parallel port of the PC, of the motors command signals, moving the end-effector along the planned trajectory**
From the previous step, we inherit the 6 vectors of the time laws of every manipulator joint.
Because of the discrete nature of step-by-step motors we converted the continuous positions to reproduce into a discrete control law of the step-by-step motors, as reported in Fig.7

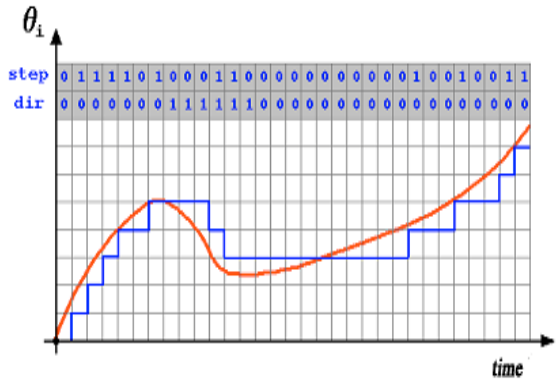


***Fig.7*** – The discreet trajectory

The overall control algorithm is summarised in the scheme of Fig.8

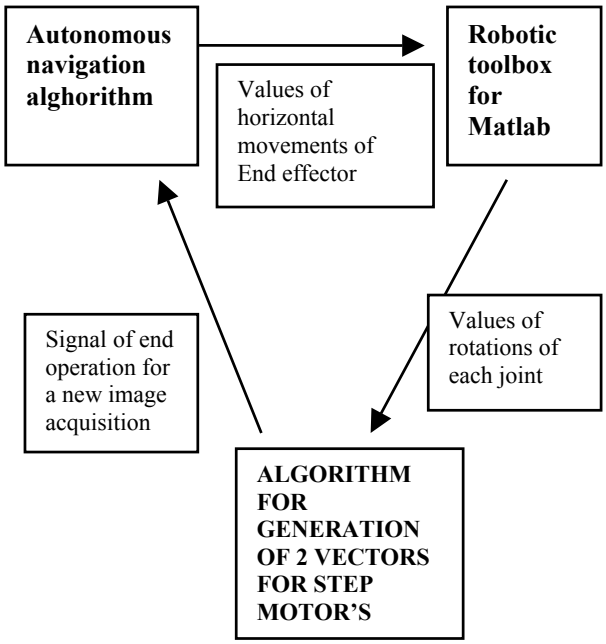


**Fig.8 -** *Autonomous control robotic arm scheme*

## 7. APPLICATION EXAMPLE

In order to validate the robotic arm and an autonomous navigation algorithm, an experiment was done. A model

of a generic celestial body surface was built and a vertical landing trajectory was simulated.
In Fig. 9 we show a landing simulation.
The robotic arm starts from a position of about 80 cm and for each step the control algorithm acquires an image, segments and searches in each image the zones suitable for landing and calculates the horizontal movements .For each step the vertical movements are fixed to simulate a constant vertical speed of landing.

**Fig. 9-** *Simulation of vertical landing*

In Fig. 10 we show the first image of landing sequence acquired from a web cam (a) and the same image segmented (b).

**Fig.10a-***First image acquired*

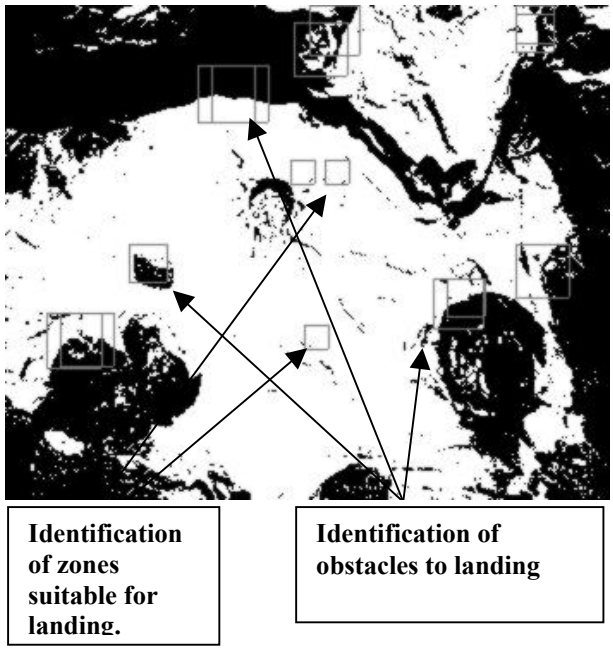


**Fig.10b-***First image segmented with the zone suitable to landing(b)*

In Fig. 11 some images extracted from the landing sequence is reported.
The images show the approach of the robotic arm to a model of a generic celestial body surface and the landmarks identified.

**Fig11a**

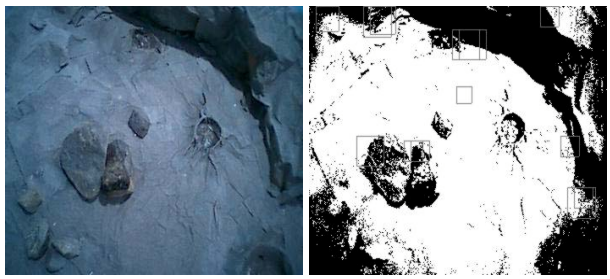

**Fig.11b**

**Fig.11c**

**Fig.11-** *Extract from the sequence of vertical landing*

### *6. CONCLUSIONS*

In this paper a robotic arm for autonomous navigation algorithm experimentation has been presented.
The vertical landing simulations are presented and the algorithm for autonomous navigation has been demonstrated to be effective and efficient in landing manoeuvres.
The main advantage of the system realized is to be able to control the end-effector movements with a videocamera and therefore it is able to verify at every cycle if the motors lost steps or if the trajectory selected is not optimal.
Some problems are due to the evaluation of the inverse kinematics with the Matlab toolbox as, the numericals solutions, generally, do not allow to determine all possible solutions, or they can determine problems for the solutions convergence.
A possible development of a robotic arm consists in the possibility of applying different tools to the end-effector for the docking or for the perforation of the ground, increasing the number of possible ground simulations of planetary exploration devices and concepts.

### REFERENCES


[1] VASILE M., ROMANO M., TRAINITI F. (1999) "An Optical Based Strategy fo Deep Space Autonomous Navigation". 4th ESA International Conference on Spacecraft Guidance, Navigation and Control Systems, ESTEC, Noordwijk 18-21 October 1999.
[2] VASILE M., STAFFIERE G.D., DAVIGHI A., FINZI A.E.(2001)" A vision system for autonomous landing manoeuvres". AIDAA- XVI Congresso Nazionale – Palermo 24-28 September 2001.
[3] CORKE P.I. (1999)" Robotics Toolbox (Release 5) for Use with Matlab"
http://www.cat.csiro.au/dmt/programs/autom/pic/matlab.html

[4] CORRADI DELL'ACQUA L. (1992) "Meccanica delle Strutture, Il Comportamento dei Mezzi Continui". McGraw-Hill.
[5] ENGDAL T." Simple 5V Power Supply for Digital Circuits".
http://www.hut.fi/Misc/Electronics/circuits/psu_5v.html
[6] Toshiba TA8435H PWM Chopper Type Bipolar Stepping Motor Driver